Experimental and Molecular Pathology 97 (2014) 154–165

Contents lists available at ScienceDirect

Experimental and Molecular Pathology

journal homepage: www.elsevier.com/locate/yexmp

CMV-induced pathology: pathway and gene–gene interaction analysis

Michael Melnick *, Krysta A. Deluca, Tina Jaskoll

Laboratory for Developmental Genetics, USC, 925 W 34th Street, Los Angeles, CA 90089-0641, USA

ARTICLE INFO

Article history:
Received 26 June 2014
Available online 28 June 2014

Keywords:
Salivary gland
Tumor microenvironment
Cell signaling
Pathway analysis

ABSTRACT

Mucoepidermoid carcinoma (MEC) is the most prevalent malignant tumor in major and minor salivary glands (SGs). We have recently identified human cytomegalovirus (hCMV) as a principle component in the multifactorial causation of SG-MEC. This finding is corroborated by the ability of the purified mouse CMV (mCMV) to induce malignant transformation of SG cells in a three-dimensional *in vitro* mouse model, using a similar oncogenic signaling pathway. Our prior studies indicate that the core tumor microenvironment (TME) is a key regulator of pathologic progression, particularly the cancer-associated fibroblast (CAF) component. Studies of early CAFs immunodetect aberrant expression of ECM components, as well as multiple growth factors, cytokines and transcription factors. Here we present the mechanistic insight derived from a mathematical structure ("wiring diagram") used to model complex relationships between a highly relevant ($p = 9.43 \times 10^{-12}$) global "cancer network" of 32 genes and their known links. Detailed characterization of the functional architecture of the examined "cancer network" exposes the critical crosstalk and compensatory pathways that limit the efficacy of targeted anti-kinase therapies.

Introduction

Salivary gland (SG) malignancies are relatively uncommon, and the prognosis is poor. Mucoepidermoid carcinoma (MEC) is the most prevalent malignant tumor in major and minor SGs (Lujan et al., 2010; Schwarz et al., 2011). We have recently identified human cytomegalovirus (hCMV) as a principle component in the multifactorial causation of SG-MEC (Melnick et al., 2012). Active hCMV protein expression positively correlates with over 90% of SG-MEC tumor cases; active hCMV also correlates and colocalizes with upregulation and activation of a well-recognized oncogenic signaling pathway (COX/AREG/EGFR/ERK).

Like other oncogenic herpesviruses [*e.g.* Epstein–Barr (Lieberman, 2014; Young and Rickinson, 2004)], the association of a rare tumor with a common virus remains puzzling. Depending on geographical and socioeconomic status, 50–95% of adults are seropositive for hCMV (Boppana and Fowler, 2007). As a herpesvirus, hCMV establishes lifelong persistence and latent infection following primary exposure (Nichols and Boeckh, 2000). Although the precise triggering mechanisms that promote hCMV reactivation in immunocompetent persons are unknown (Yuan et al., 2009), Dağ et al. (2014) have now shown that reversible silencing of CMV genomes by type I interferon governs viral latency. Further, of particular interest here, hCMV, both active and latent, has a special tropism for SGs (Nichols and Boeckh, 2000; Wagner et al., 1996).

That human SG-MEC is highly correlated with active hCMV is corroborated by the ability of purified mouse CMV (mCMV) to induce malignant transformation of SG cells in an *in vitro* mouse model, using a similar oncogenic signaling pathway (Jaskoll et al., 2011; Melnick et al., 2011, 2013a, 2013b). This novel SG organ culture model provides an ideal system for investigating CMV-induced dysregulation of multiple host cell signaling pathways, focusing on a network of interactions between genes and pathology. Moreover, since the three-dimensional associations between acinar, ductal and stromal cells are maintained, this postnatal SG organ culture permits delineation of the cell-specific localization of important molecules with progressive infection and identifies initiating and sustaining pathway components in a variety of cell types, thus providing evidence for the pathophysiologic relevance of these components (dysregulation → neoplasia).

Presently, it is well-argued that the core tumor microenvironment (TME) ("stroma") is integral to cancer initiation, growth and progression (Cortez et al., 2014; Hanahan, 2014; Hanahan and Coussens, 2012; Heldin, 2013; Marsh et al., 2013; Pietras and Ostman, 2010). In particular, tumor evolution is promoted by "transformed" stromal fibroblasts that are now termed cancer-associated fibroblasts (CAFs). CAFs actively drive tumorigenesis and progression by paracrine and juxtacrine crosstalk between fibroblasts and between CAFs and epithelium, using canonical growth factor and cytokine pathways (*e.g.* EGFR, FGFR, IL-6). Notwithstanding, the function of CAFs in *de novo* induction of carcinoma in epithelium lacking oncogenic mutation is controversial (Marsh et al., 2013).

* Corresponding author at: Laboratory for Developmental Genetics, University of Southern California, 925 W 34th Street, DEN 4266, MC-0641, Los Angeles, CA 90089-0641, USA.
E-mail addresses: mmelnick@usc.edu (M. Melnick), krysta.arwen@gmail.com (K.A. Deluca), tjaskoll@usc.edu (T. Jaskoll).

http://dx.doi.org/10.1016/j.yexmp.2014.06.011
0014-4800/

Our prior studies routinely suggest that early in CMV-induced SG tumorigenesis, the core TME is a key regulator of pathologic progression, particularly the CAF component (Jaskoll et al., 2011; Melnick et al., 2013a, 2013b). Although the stroma is densely populated with giant basophilic round cells mixed with far fewer and smaller eosinophilic cells, only a subset of CAFs are infected; the remainder are affected (Fig. 1). Regarding SG epithelia, none of the cells are infected early on, though there are some signs of early dysplasia, such as pseudostratified ductal epithelia and dilated lumina filled with cellular debris (Fig. 1).

Of note, our initial studies of early CAFs immunodetect aberrant expression of ECM components, as well as several growth factors, cytokines and transcription factors (Melnick et al., 2011, 2013a, 2013b). How might these and other sentinel gene products regulating cell proliferation and survival relate to one another as components of a larger network? Are the gene expressions and relationships pathognomonic of malignant tumorigenesis? What mechanistic insight can be derived from a mathematical structure ("wiring diagram") used to model complex relationships between a finite set of genes (nodes) with known links (edges)? What therapeutic opportunities emerge from the revealed causal network? These critical questions are addressed here using systems analysis of a defined network.

Materials and methods

Animals

Timed pregnant inbred C57/BL6 female mice (Charles River, Wilmington, MA) were purchased from Harlan Laboratories (Indianapolis, IN) (plug day = day 0 of gestation) and newborn (NB) mice were harvested as previously described (Melnick et al., 2006, 2009). All protocols involving mice were approved by the Institutional Animal Care and Use Committee (USC, Los Angeles, CA).

Organ culture

Newborn submandibular glands (SGs) were dissected and cultured for 6 or 12 days using a modified organ culture Trowell method and BGJb media (Invitrogen Corporation, Carlsbad, CA) as previously described (Melnick et al., 2006, 2011). For mCMV infection, SGs were incubated with 1×10^5 plaque-forming units (PFU)/ml of *lacZ*-tagged mCMV RM427+ in BGJb on day 0 for 24 h and then cultured in virus-free media for a total culture period of 6 or 12 days; controls consisted of SGs cultured in control media for the entire period. For all experiments, media were changed daily. SGs were collected and processed for hematoxylin and eosin histology, immunolocalization, and qRT-PCR. For histology, and immunolocalization analysis, SGs were fixed for 4 h at 4 °C in Carnoy's fixative or 10% neutral buffered formalin, embedded in low melting point paraplast, serially-sectioned at 8 μm and stained as previously described (Melnick et al., 2006).

To obtain a measure of mCMV infection, we assayed for β-galactosidase (*lacZ*) activity essentially as previously described (Melnick et al., 2006). β-Galactosidase-stained whole mounts were then dehydrated through graded alcohols, embedded in paraffin, serially-sectioned and counterstained with eosin.

Immunolocalization

Cultured SGs were serially-sectioned at 8 μm and immunostained as previously described (Melnick et al., 2006, 2009) using the following commercially-available polyclonal antibodies: Amphiregulin (sc-25436); β-catenin (sc-7199); pERK1/2 (Thr202/Tyr204) (sc-

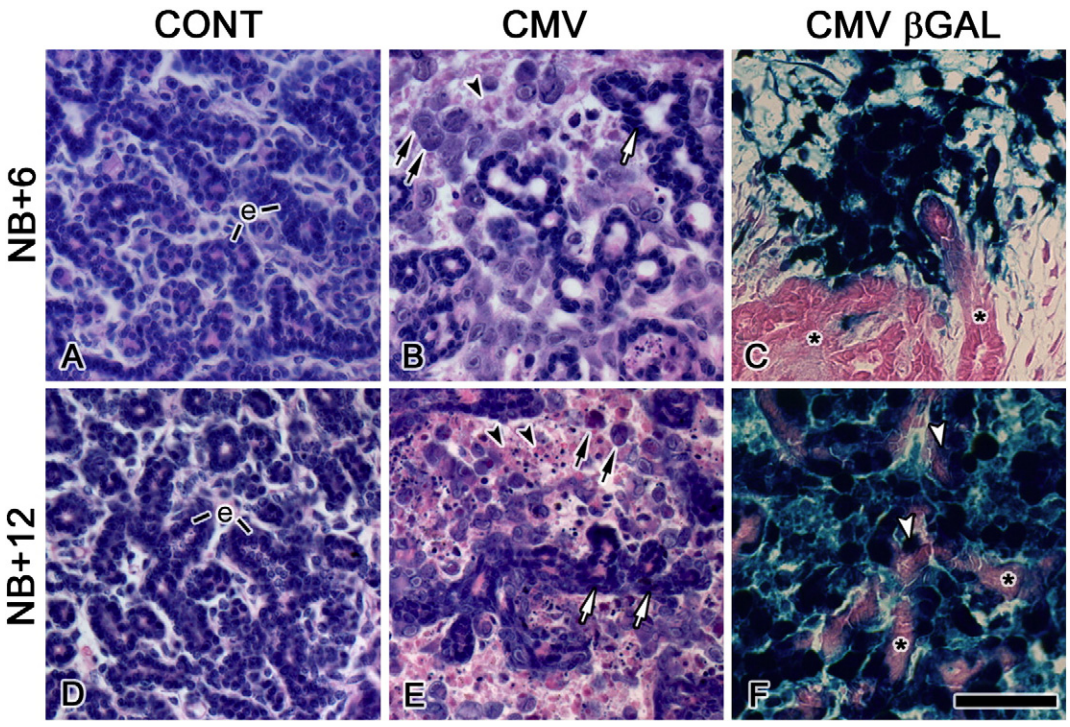

Fig. 1. mCMV infection induces a severe cytopathic effect in SG stroma. A–C. NB + 6 SGs. D–F. NB + 12 SGs. Control SGs (A, D) are characterized by densely packed, branched cuboidal ductal and pro-acinar epithelia (e) surrounded by a fibromyxoid stroma. mCMV-infected SGs (B, E) exhibit epithelial dysplasia (white arrow) and significant viral cytopathic effect in the stroma, with greater viral-induced histopathology seen on day 12 than on day 6 (compare E to B). The abnormal epithelia are embedded in a hypercellular stroma composed of large basophilic, pleiomorphic cells (black arrows) and smaller eosinophilic cells (black arrowheads), with frequent kidney-shaped nuclei pathognomonic of CMV infection being seen. C, F. β-Galactosidase-stained mCMV is distributed in abnormal stroma, with a marked increase being seen on day 12 (compare F to C). Note that β-galactosidase-stained virus is mostly absent in eosin-stained epithelia (*) on day 6 (C) but present in epithelia on day 12 (white arrowheads) (compare F to C). Bar, 30 μm.

16982); pEGFR (Tyr 1173) (sc-101668); FGFR3 (sc-123); SHH (sc-9024) (Santa Cruz Biotechnology, Inc., Santa Cruz, CA); and FGF8 (PAB12306) (Abnova, Taipei, Taiwan). Nuclei were counterstained with DAPI (Invitrogen Corporation). Negative controls were performed in parallel under identical conditions and consisted of sections incubated without primary antibodies. For each treatment group, 3–6 SGs per day/antibody were analyzed. All images were acquired with a Zeiss Axioplan microscope equipped with a SPOT RT3 camera and processed with SPOT Advanced and Adobe Photoshop CS2 software.

For PCNA (proliferating cell nuclear antigen) localization, we conducted immunohistochemistry using the Zymed mouse PCNA kit (Invitrogen Corporation) and counterstained with hematoxylin and eosin essentially as previously described (Melnick et al., 2006). In this set of experiments, PCNA-positive nuclei appear dark brown.

Interruption studies

To interrupt EGFR signaling, we used 10 μM gefitinib (GEF) (Selleck Chemicals LLC, Houston, TX), a small molecule inhibitor which blocks the binding of ATP to the intracellular TK domain of EGFR. This concentration was previously determined to be the optimal dose (Melnick et al., 2011). NB SGs were infected with 1×10^5 PFU/ml mCMV for 24 h in the presence or absence of 10 μM GEF and then cultured in control medium with or without GEF for a total of 12 days; controls consisted of glands cultured in control medium or control medium + GEF for the entire 12 days. *For co-targeting inhibition of the EGF/ERK signaling*, we used 10 μM U0126 (EMD Chemicals, Inc., Gibbstown, NJ), a potent and specific inhibitor of MEK-mediated ERK1 and ERK2 phosphorylation, concurrently with GEF treatment beginning at day 6. This concentration of U0126 was previously determined to be the optimal dose (Melnick et al., 2011). NB SGs were infected with 1×10^5 PFU/ml mCMV for 24 h in the presence or absence of 10 μM GEF and then in control medium ± inhibitor. Beginning on day 6, we additionally added 10 μM U0126 (GEF + D6U) to the culture medium for an additional 6 days (a total culture period of 12 days). Controls consisted of untreated, GEF-treated, or GEF + D6U-treated SGs. Media were changed and inhibitors were added daily. No differences between treatment groups were seen; untreated controls are presented. In this experiment, a minimum of 3 explants per treatment per antibody were analyzed.

Quantitative RT-PCR

For analysis of gene expression, qRT-PCR was conducted as previously described (Melnick et al., 2006, 2009) on NB + 6 control and mCMV-infected samples; each sample consisted of 4–5 pooled explants. RNA was extracted and 1 μg RNA was reverse transcribed into first strand cDNA using ReactionReady™ First Strand cDNA Synthesis Kit: C-01 for reverse transcription (Qiagen, Germantown, MD). The primer sets used were prevalidated to give single amplicons and purchased from Qiagen: Areg (PPM02976A); Bcl2 (PPM02918A); Cadherin1 (PPM03652A); Casp3 (PPM02922A); Ctnnb (β-catenin) (PPM03384A); Egf (PPM03703A); Egfr (PPM03714A); Fgf8 (PM02962A); Fn1 (PPM03786A); Gapdh (PPM02946A); Gli1 (PPM41530A); Gli3 (PPM25249A); Itga5 (PPM03609A); Itgb1 (PPM03668A); Il6 (PPM03015A); Lef1 (PPM05441A); Mapk3 (ERK1) (PPM03585A); (Mapk8) (JNK1) (PPM03234A); Mdm2 (PPM02929A); Myc (PPM02929A); NFKb1 (PPM02930A); Nfkb2 (PPM03204A); Pcna (PPM03456A); Pdgfra (PPM03640A); Pik3r1 (PPM03374A); Ptgs2 (Cox2) (PPM03647A); Rela (PPM42224A); Relb (PPM03202A); Shh (PPM04516A); Stat3 (PPM04643A); Tgfa (PPM03051A); Tnfa (PPM03113A); Trp53 (p53) (PPM02931A). Primers were used at a concentration of 0.4 μM. The cycling parameters were 95 °C, 15 min; 40 cycles of (95 °C, 15 s; 55 °C, 30–40 s and 72 °C, 30 s). Specificity of the reactions was determined by subsequent melting curve analysis. RT-PCRs of RNA (not reverse transcribed) were used as negative controls. GAPDH was used to control for equal cDNA inputs and the levels of PCR product were expressed as a function of GAPDH. The relative fold changes of gene expression between the gene of interest and GAPDH, or between the NB + 6 control and mCMV-infected samples, were calculated by the $2^{-\Delta\Delta CT}$ method. Significant expression differences between mCMV-infected and control samples were determined by Student's t-test, with $\alpha = 0.01$ and the null hypothesis of $R = 1$, where R is the mean relative expression ration (mCMV/control) across the entire sample. Expression ratios were log transformed prior to analysis to satisfy the assumption of normality.

Pathway and gene–gene interaction analysis

Ingenuity Pathway Analysis (IPA, QIAGEN Redwood City, www.qiagen.com/ingenuity) tools were used to analyze possible functional relationships between 32 genes (focus molecules), using inputs of gene identifiers, $\log_2$ fold-changes, and p-values between mCMV-infected and uninfected control glands. Networks of these focus molecules were then algorithmically generated based on their connectivity, disease, and canonical pathways, and molecular and cellular functions were then ranked by score. The score associated with a particular network is the likelihood of the genes identified as differentially expressed in a network being found together by chance. In the canonical pathway analysis, the canonical pathways that were most significant to the 32 genes were identified and p value determined by the IPA tool. The image was generated from IPA software using the canonical pathways feature, network builder feature, and path designer tools.

Table 1
Gene expression.

Gene	Δ	p	D
AREG	2.08	<0.01	↑
EGFR	0.86	<0.01	↓
TGFα	0.78	<0.01	↓
EGF	0.79	>0.05	–
ERK1	0.79	<0.01	↓
cMyc	0.85	<0.01	↓
FGF8	2.43	<0.001	↑
PDGFRα	0.94	>0.05	–
PI3K	0.97	>0.05	–
NFκB1	0.71	<0.01	↓
NFκB2	0.95	>0.05	–
RelA	0.88	<0.01	↓
RelB	0.89	<0.01	↓
TNFα	1.55	<0.01	↑
IL-6	6.51	<0.01	↑
STAT3	1.08	>0.05	–
JNK1	0.83	<0.01	↓
MDM2	1.21	<0.05	↑
p53	0.88	<0.01	↓
Casp3	1.22	<0.02	↑
Bcl2	0.60	<0.001	↓
PCNA	1.20	<0.02	↑
Cadherin1	0.81	<0.01	↓
COX2	6.36	<0.01	↑
FN1	1.44	<0.01	↑
Int β1	0.83	<0.01	↓
Int α5	1.31	<0.02	↑
β-Catenin	0.93	<0.05	↓
Lef1	1.51	<0.01	↑
SHH	3.57	<0.001	↑
Gli1	1.31	>0.05	–
Gli3	1.34	<0.01	↑

Δ = mean $\log_2$ change across all samples (n = 9), *i.e.* the mean increase or decrease in gene expression in CMV-treated SGs compared to SG controls.
p = statistical significance.
D = direction of change, up (↑) or down (↓) or none (–).

Results

Based on the long-recognized molecular and cellular homologies between tumorigenesis and organogenesis (Egeblad et al., 2010; Huang, 2011; Wiseman and Werb, 2002), and our extensive studies of salivary gland (SG) ontogenesis (*e.g.* Jaskoll et al., 2004a, 2004b, 2005; Melnick and Jaskoll, 2000), we utilized network modeling to investigate 32 probative genes (Table 1) in signaling pathways that are both participants in CMV-induced tumorigenesis (Jaskoll et al., 2011; Melnick et al., 2011, 2013a, 2013b) and share post-activation downstream targets: Egfr, Fgfr, Il6r, Tnfr, Shh, and β-catenin (Ctnnb1). Network thinking provides the ability to simplify complex problems without losing their essential features. Because this approach is experimentally constrained and computationally accessible, it is heuristically very useful (Giuliani et al., 2014). Indeed, below we present novel emergent properties that would not be otherwise evident.

We determined the expression of 32 genes in mCMV-treated SGs after 6 days of infection (NB + 6), a time when the core TME appears to be a key regulator of pathologic progression, particularly the "transformed" stromal fibroblasts (CAFs) (Fig. 1) (Jaskoll et al., 2011; Melnick et al., 2011, 2013a, 2013b). The analytical results of quantitative RT-PCR (qRT-PCR) are presented in Table 1. Remarkably, 26 of the 32

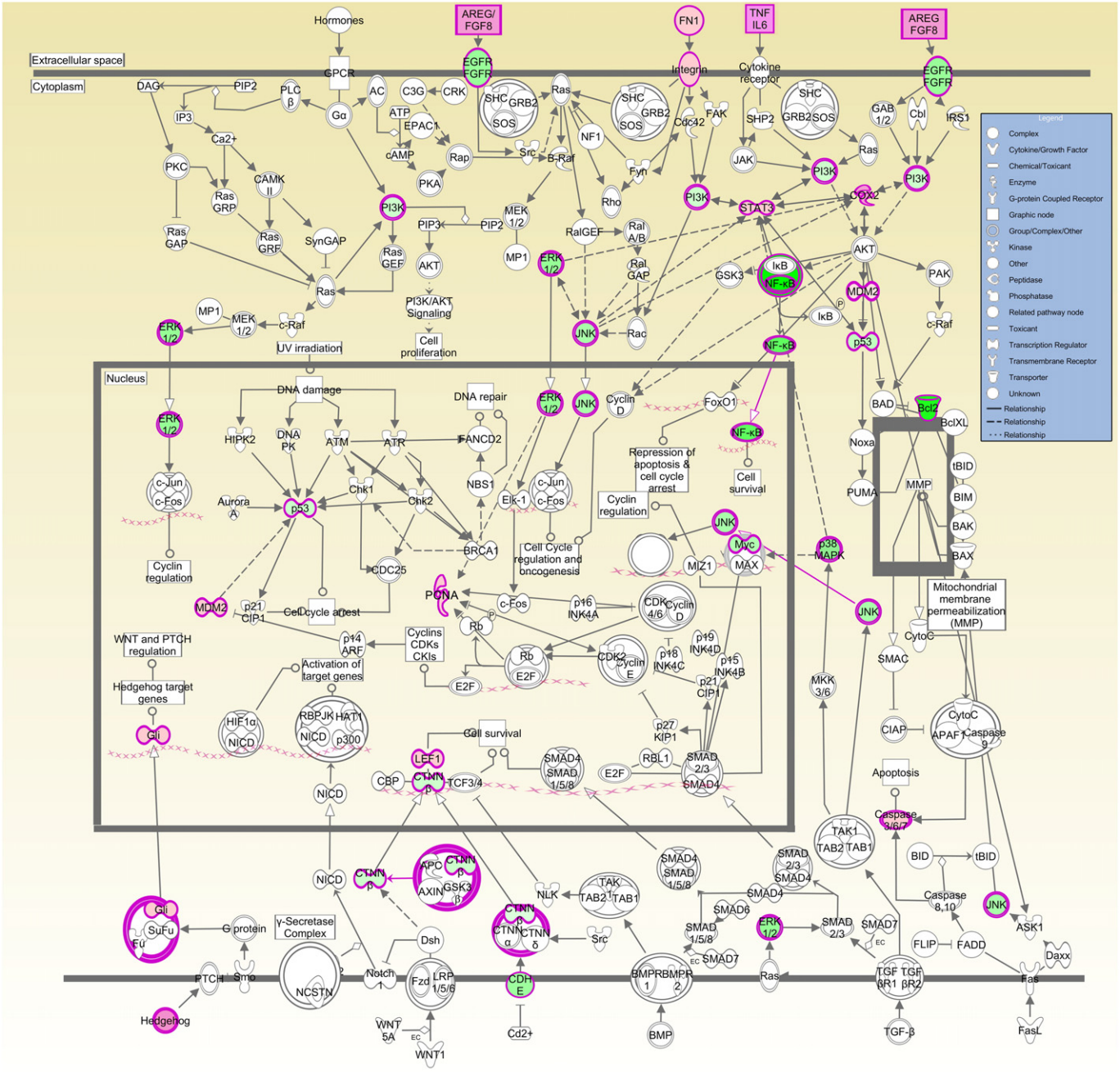

Fig. 2. Canonical pathway implicated in cancer pathogenesis. A data set containing the differentially regulated genes between mCMV-infected and control NB + 6 SGs was overlaid onto a global canonical network showing the mechanism of cancer. The magenta highlighted molecules indicate genes whose expression was altered by mCMV infection compared to control. Pink-colored shapes denote upregulated genes and green colored shapes denote downregulated genes; the darker the color, the greater the change. The nodes are displayed using various shapes that represent the functional class of gene product (image was generated from IPA software using the canonical pathways feature and the path designer tool)

had significant $\log_2$ fold changes relative to uninfected controls. In typical fashion, these genes may be viewed in a "cancer map" (Fig. 2) as a series of related linear pathways in which initial signaling events (aberrant or not) progressively amplify after a sequence of Boolean choices to emerge at end-points that we term cell proliferation, cell survival, cell cycle arrest, apoptosis, *etc.* While this may provide a broad view, it allows only an imagined dynamic understanding.

The nonlinear complexity of living systems is largely due to networks of genes rather than the sum of independent effects of individual genetic pathways. Thus, we have always to focus on the relationship between genes/pathways, rather than the genes/pathways themselves. This is so because the complexities of tumorigenesis largely emerge from complexities in the interactions of genes within and among cells. Using the qRT-PCR data (Table 1), we undertook a comprehensive network and pathway analysis utilizing Ingenuity Pathway Analysis (IPA), as well as other statistical approaches.

Fig. 3 represents the 32 genes (nodes) and their known functional links (edges) between them; this iteration highlights nearest neighbors. This network has several important features. First, the calculated probability that this specific qRT-PCR data set is from carcinoma is highly significant ($p = 9.43 \times 10^{-12}$), as it is for head and neck cancer ($p = 7.06 \times 10^{-16}$). Second, the network has a classic small world property, namely the short paths between most pairs of nodes (genes) and relatively few "long-distance" links. Finally, there is considerable clustering, the extent to which a gene's nearest neighbors are also neighbors to each other, forming communities.

Because of the therapeutic implications, one such community is of particular interest to us: EGFR, FGFR, FGF8, SHH, β-catenin, ERK1, and PCNA. Numerous studies in recent years have made it clear that there is an intimate functional relationship between their respective pathways (Fig. 4). Of particular importance, while EGFR signaling is dominant to FGFR signaling (*via* the ERK pathway), EGFR and FGFR provide mutual "escape" mechanisms from respective small molecule inhibition. This may be a plausible explanation for the *in vitro* and *in vivo* failure of therapeutic interventions with drugs such as gefitinib (*e.g.* Jakob et al., 2014; Robinson and Sandler, 2013; Ware et al., 2013).

Analysis of the IPA-constructed aforementioned community (Fig. 5) reveals key functional characteristics. It is a canonical small-world subnetwork (Watts and Strogatz, 1998): (a) short path lengths (L) between pairs of nodes (genes); (b) a mean node degree (number of links in and/or out of a node) of 4.63, consistent with the existence of hubs ($d \geq 5$); (c) at 0.71, the Clustering Coefficient (C) indicates that this is a "tight-knit" community (for any genes x, y and z, if gene x is linked to genes y and z, then y and z are also linked to each other).

High degree nodes are termed hubs, *a priori* primary channels of information flow. There are 4 genes with a degree (d) greater than or equal to 5 (Fig. 5): EGFR, β-catenin, FGF8, and SHH. For each hub, we calculated the average Pearson correlation coefficients (PCCs) between the hub and each of its respective partners for mRNA expression (as per Han et al., 2004). Hubs with mean PCCs of 0.5 or more are termed "party hubs" and those less than 0.5 are termed "date hubs"; party hubs correspond to more permanent interaction, while date hubs correspond to transient interactions (Han et al., 2004). All 4 network hubs are date hubs: EGFR ($\bar{r} = 0.4043$); β-catenin ($\bar{r} = 0.4038$); FGF8 ($\bar{r} = 0.4975$); SHH ($\bar{r} = 0.4561$). Genetic dysregulation of date hubs tends to sensitize the larger network (Figs. 2, 3) to other dysregulations, more so than party hubs (Han et al., 2004). This has important, and challenging, therapeutic implications.

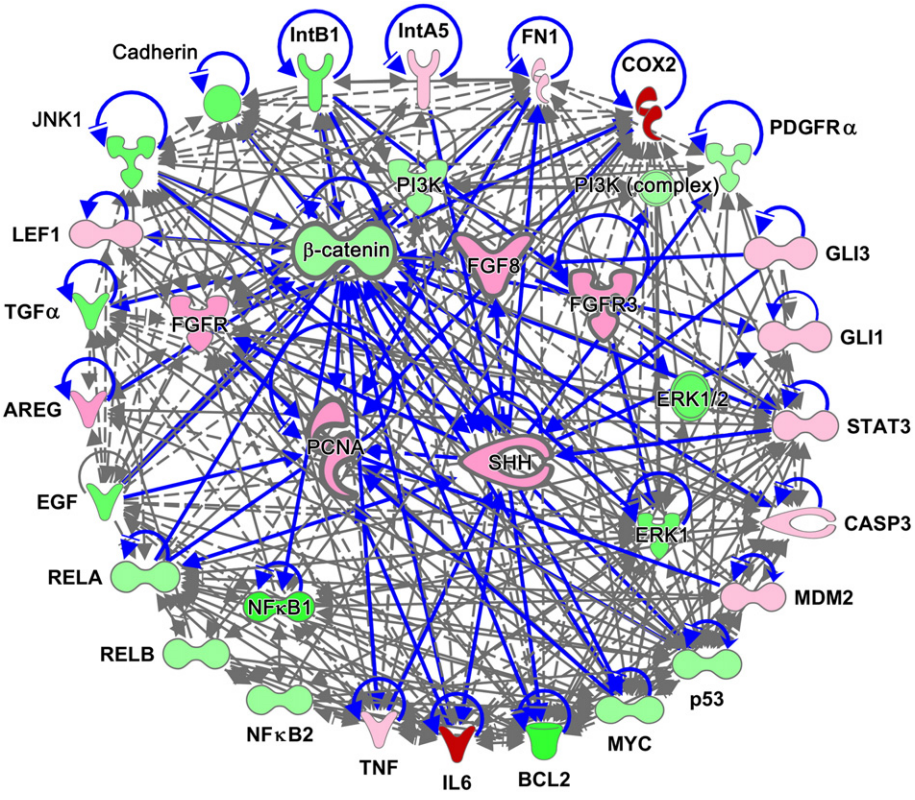

Fig. 3. Mechanistic network analysis by IPA of the expression of 32 genes (nodes) and their known functional links (edges) in mCMV-infected NB + 6 SGs compared to control SGs. A small-world network showing the functional relationships between the 32 genes and highlighting their nearest neighbors. Red-colored shapes denote upregulated genes and green colored shapes denote downregulated genes; the darker the color, the greater the change. The nodes are displayed using various shapes that represent the functional class of gene product and the style of the lines connecting the molecules indicates specific molecular relationships and the direction of the interaction.

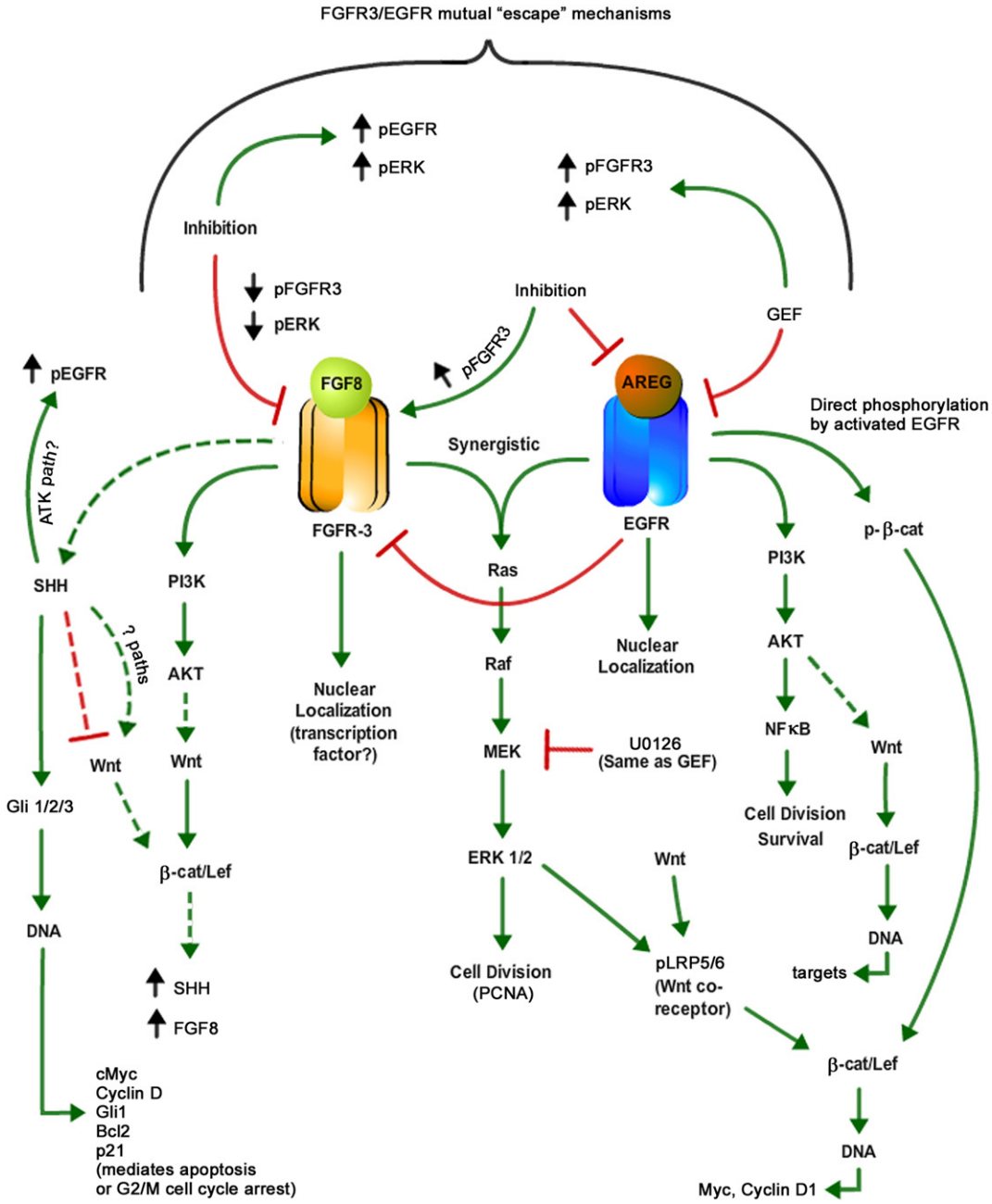

Fig. 4. Putative functional relationship between EGFR, FGF8, FGFR3, SHH, β-catenin, ERK1 and PCNA. References: Akiyama et al. (2014), Bigelow et al. (2005), Cerliani et al. (2012), Degnin et al. (2011), Eswarakumar et al. (2005), Götschel et al. (2013), Hai et al. (2010), Herrera-Abreu et al. (2013), Ho et al. (2014), Issa et al. (2013), Iwatsuki et al. (2007), Johnston et al. (1995), Katoh and Katoh (2008), Kono et al. (2009), Krejci et al. (2012), Marshall et al. (2011), Mavila et al. (2012), Oliveras-Ferraros et al. (2012), Patel et al. (2011), Reid et al. (2011), Reinchisi et al. (2013), Sinor-Anderson and Lillien (2011), Su et al. (2012), Sütterlin et al. (2013), Wang et al. (2011, 2012), Ware et al. (2010, 2013), Zammit et al. (2001).

Fibroblasts comprise the major cell type within the TME of most carcinomas, and are thought of as "architects of cancer pathogenesis" (Marsh et al., 2013). Hanahan (2014) makes the case that "counterattacking" a cancer should begin at the site where the cancer emerged, the core TME. Within the context of the community (cluster) of interest (Fig. 5), we have used immunohistology to define the core TME protein signature of CMV-induced tumorigenesis (Figs. 6, 7).

We determined the cell-specific localization of AREG and its cognate receptor EGFR, FGF8 and its cognate receptor FGFR3, activated (phosphorylated) ERK1/2 (pERK1/2), SHH, β-catenin and PCNA, a marker of cell proliferation, in mCMV-infected and uninfected SG organs *in vitro* (Fig. 6–7). At 6 days of infection (NB + 6) (Fig. 6), there is a notable increase in immunolocalized AREG, FGF8, activated (nuclear-localized) FGFR3, activated (phosphorylated) EGFR (pEGFR), pERK1/2, SHH, and β-catenin compared to controls (Fig. 6), with all proteins primarily detected in the cytomegalic stromal cells. Of particular interest is the abundance of nuclear-localized (activated) FGFR3 throughout the TME in mCMV-infected SGs. In contrast, controls exhibit membrane-localized FGFR3 on a subset of epithelial cells (compare Figs. 6H to G). In addition, we also detected a marked increase in nuclear-localized PCNA in mCMV-infected SGs compared to control SGs, as well as notable differences in its cell-specific localization (compare Figs. 6P to O). mCMV-infected SGs are characterized by nuclear-localized PCNA throughout cytomegalic stromal cells (Fig. 6O); in controls, only a few cells exhibit nuclear-localized PCNA, primarily being found in ductal and acinar epithelial cells (compare Figs. 6P to O).

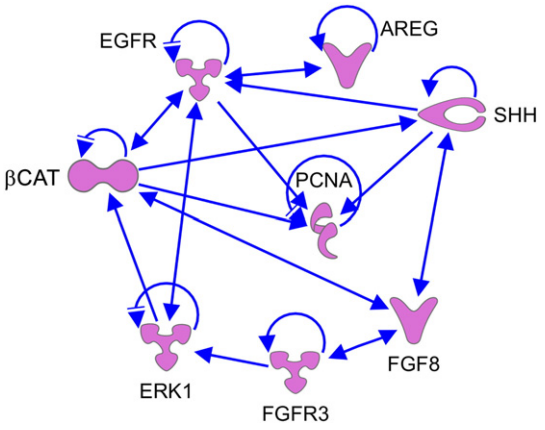

Fig. 5. Functional network analysis of AREG, EGFR, FGF8, FGFR3, β-catenin, ERK1, SHH and PCNA. Network analysis using IPA tools was conducted on the 8 differentially expressed genes of interest and their close relationships shown. The nodes are displayed using various shapes that represent the functional class of gene product (*e.g.* protein family). The style of the lines connecting the molecules indicates specific molecular relationships and the direction of the interaction.

mCMV-infected SGs cultured for 12 days (NB + 12) exhibit a more severe viral cytopathic effect in the stroma, and abnormal parenchyma consistent with a tumorigenic phenotype (Fig. 1E). The marked increased stromal cellularity is composed of sheets of large basophilic, pleomorphic cells and smaller eosinophilic cells with prominent nuclei and nucleoli, and high nuclear-to-cytoplasm ratios. The increasingly sparse epithelia are characterized by increased nuclear-to-cytoplasm ratios, hyperchromatism and visible nucleoli; intraluminal proliferation and extrabasal proliferation impart a multilayered appearance to these epithelial islands. At 12 days, both stroma and epithelia are well-infected with mCMV (Fig. 1F). The protein signature reflects the progressive pathogenesis (Fig. 7). The marked increase in immunodetectable AREG, pEGFR, FGF8, activated FGFR3, pERK, SHH, and β-catenin, as well as substantial differences in their cell-specific localization, persist in NB + 12 mCMV-infected SGs compared to uninfected control SGs (Fig. 7). All proteins are found throughout the TME in mCMV-infected SGs. In addition, nuclear-localized PCNA is seen in most, if not all, cytomegalic stromal cells in mCMV-infected SGs but is relatively absent in control SGs (compare Figs. 7P to O).

Relationship between EGFR and FGFR signaling

We have previously reported that inhibitors of the EGFR → ERK pathway do not fully rescue well-established mCMV-induced SG pathology, either singly or in combination, and suggested that CMV induces alternative signaling pathways that promote and maintain downstream cell proliferation and survival (*i.e.* SG pathology) (Melnick et al., 2013a, 2013b; Fig. 4). Herein, we focused on the relationship between EGFR and FGFR3 signaling purported in the literature (Fig. 4). We treated mCMV-infected SGs *in vitro* with gefitinib (GEF), an EGFR inhibitor, with/without an inhibitor of MEK-mediated, ERK phosphorylation (U0126).

Treatment with GEF (CMV + GEF) for the entire 12-day culture period results in only a marginal reduction in immunodetectable FGF8 and activated (nuclear-localized) FGFR3, albeit with a marked increase in membrane-localized FGFR3 (Fig. 8G), compared to untreated mCMV-infected SGs (compare Figs. 8E to 7F, 8G to 7H). However, the expression patterns of pERK, SHH, β-catenin, and PCNA are similar in GEF-treated and untreated mCMV-infected SGs (compare Figs. 8I to 7J, 8K to 7L, 8M to 7N, 8O to 7P). Our demonstration of nuclear-localized FGFR3 suggests that FGF8/FGFR3 signaling continues to activate key downstream targets and promotes cell proliferation in the absence of EGFR signaling.

We then inhibited EGFR *and* ERK signaling with the addition of the ERK inhibitor U0126, beginning on day 6, to GEF-treated, mCMV-infected SGs (CMV + GEF + D6U). With inhibition of the EGFR → ERK pathway, we noted the absence of nuclear-localized FGFR3 (compare Figs. 8H to 7H, 8G); the membrane-localized FGFR3 expression pattern is similar to that seen in controls (compare Figs. 8H to 7G). This unexpected change in FGFR3 localization is associated with epithelial morphologic improvement, reduced TME pathology, and a marked decrease in cell proliferation (compare Figs. 8P to 6P, 7P, and 8O). Concomitantly, the patterns of pERK, SHH and β-catenin expression only slightly differ from those seen with GEF treatment alone (compare Figs. 8J to I, L to K, N to M) or untreated mCMV-infected SGs (compare Figs. 8J to 7J, 8L to 7L, 8N to 7N) and likely contribute to the viral-induced pathology still found in these SGs.

Discussion

While the role of fibroblasts in *de novo* transformation or induction of carcinoma in epithelia lacking oncogenic mutation is vigorously debated (Hanahan, 2014; Marsh et al., 2013; Pietras and Ostman, 2010), our mouse model clearly demonstrates that CMV subverts resident SG fibroblasts to initiate and promote SG epithelial tumorigenesis (Figs. 1, 6, 7). Thus, they are properly referred to as cancer-associated fibroblasts (CAFs). CAFs directly stimulate (initiate) epithelial transformation and tumor cell proliferation *via* growth factors and cytokines acting in a paracrine or juxtacrine manner within the context of a remodeled extracellular matrix (Cortez et al., 2014; Hanahan, 2014; Marsh et al., 2013). We have identified a core TME protein signature of "driver dysregulation" that is relatively stable through progressive pathogenesis (Figs. 6, 7). This "community" of gene products has important properties: each protein is not an independent actor, and as such, therapeutic intervention is until now daunting (*e.g.* Engelman and Settleman, 2008; Melnick et al., 2013a; Wilson et al., 2012).

Emergent biologic phenomena (*e.g.* cancer) are both multifactorial and unable to be predicted from functional knowledge of individual components. To understand pathogenesis, as one example, it must be modeled within the context of organized networks that are measurable at both local and global network scales (Aderem et al., 2011; Mora et al., 2014). Here we present a highly relevant ($p = 9.43 \times 10^{-12}$) global "cancer" network of 32 genes (nodes) and their known links (Fig. 3). Within such a network is a subset of nodes (genes) designated "driver nodes," defined as genes capable of controlling the entire network when they are driven by external signals (Onnela, 2014). In other words, controlling a complex directed network (such as that in Fig. 3) reduces to the selection of specific nodes that, by virtue of being directly controlled (*e.g.* dysregulated by CMV), can indirectly drive the rest of the network to an emergent state (*e.g.* tumorigenesis) (Ruths and Ruths, 2014).

Global networks such as that in Fig. 3 contain multiple smaller "tight-knit" communities with clustering coefficients approaching unity. Here we focus on one such local subnetwork (Fig. 5) of therapeutic importance. Like most transcriptomic networks, it is dominated by external dilations, *i.e.* paths that split without subsequently rejoining (Figs. 4, 5) (Ruths and Ruths, 2014). The subnetwork has multiple sink nodes (*e.g.* ERK1, PCNA) and correlated behaviors across the upstream agents that are downstream from a common source (date hubs). Detailed characterization of the functional architecture of the examined "cancer network" (Figs. 3–5) is critical because crosstalk and compensatory pathways (Fig. 4) in such networks limit the efficacy of targeted anti-kinase therapies (Kirouac et al., 2013; Melnick et al., 2013a, 2013b). This is again evidenced in our study of the functional FGFR3/EGFR relationship using small molecule inhibitors (Fig. 8); other members of the dynamic network (Fig. 3, 5) continue to assert themselves (Fig. 8) in a dysfunctional manner associated with SG pathology.

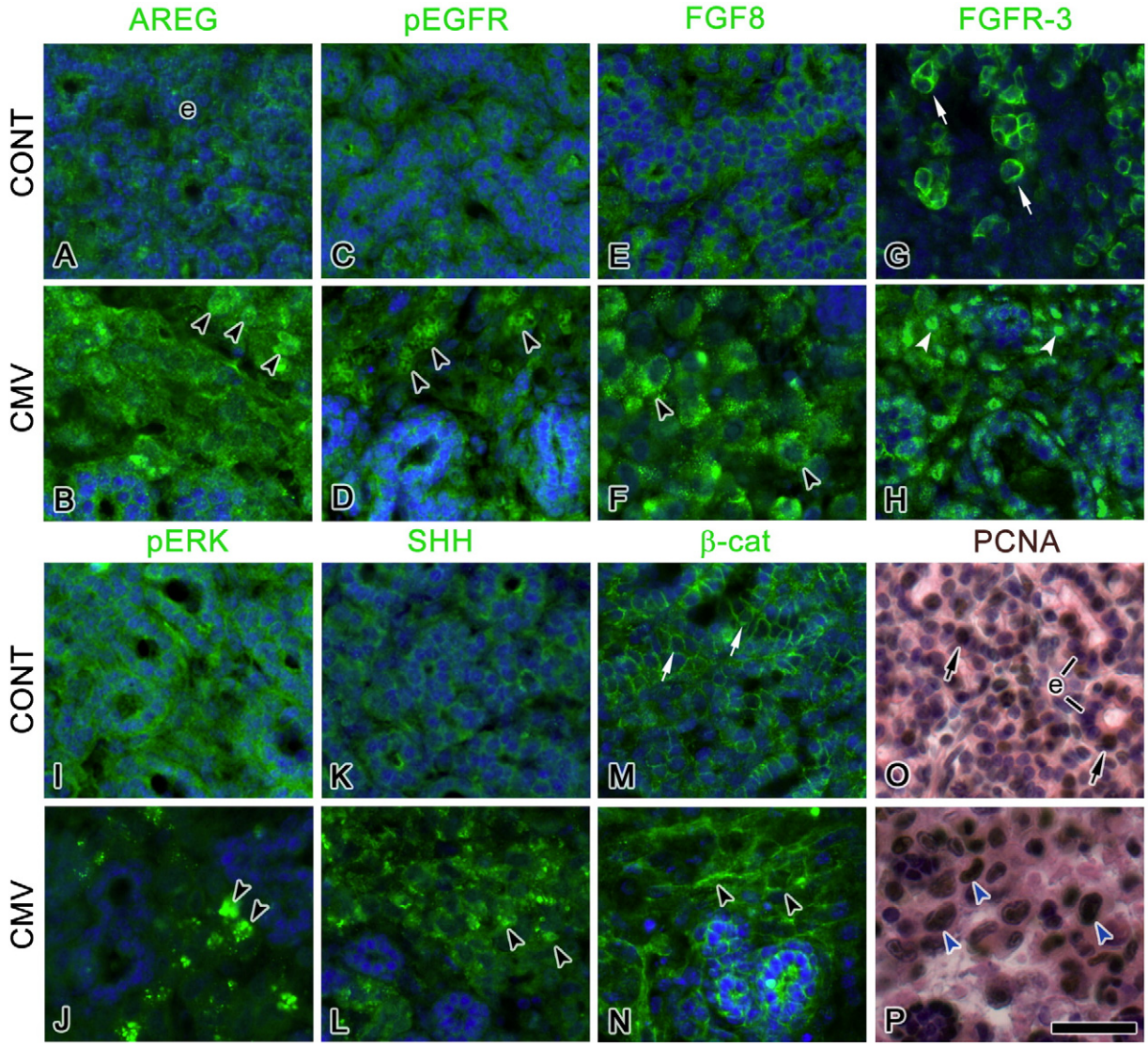

Fig. 6. CMV-induced stromal localization of components of the AREG/EGFR and FGF8/FGFR3 signaling pathways in NB + 6 SGs. A–D. AREG and EGFR expression. In mCMV-infected SGs, AREG (B) and activated (phosphorylated) pEGFR (D) are localized in cytomegalic stromal cells (black arrowheads) but are relatively absent from control epithelia (e) and stroma (compare B to A, D to C). E–H. FGF8 and FGFR3 expression. In mCMV-infected SGs, FGF8 (F) and nuclear-localized FGFR3 (H, white arrowheads) are found throughout abnormal stroma; membrane localized FGFR3 is also found in a small number of epithelial cells (data not shown). In contrast, controls are characterized by the relative absence of FGF8 (E) and the presence of membrane-localized FGFR3 (G, white arrows) on a subset of epithelial cells. I–J. pERK expression. In mCMV-infected SGs (J), pERK is immunolocalized in a subset of cytomegalic stromal cells and is relatively absent in controls (I). K–L. SHH expression. In mCMV-infected SGs (L), SHH is detected throughout abnormal stroma, and is weakly seen on control epithelia (K). M–N. β-Catenin expression. In controls, β-catenin is seen on epithelial cell membranes (M, white arrows); with mCMV-infection (N), β-catenin is primarily found on abnormal stromal cell membranes (black arrowheads). O–P. PCNA expression. In controls (O), nuclear-localized PCNA (brown color) is infrequently seen, primarily being detected in a few epithelial cells (black arrows). In mCMV-infected SGs (P), nuclear-localized PCNA is seen in the majority of abnormal cytomegalic stromal cells. Note the presence of nuclear-localized PCNA in cells exhibiting kidney-shaped nuclei pathognomonic of viral infection (blue arrowheads). DAPI-stained nuclei appear blue. Bar, 50 μm.

Conclusions

Structural network modeling is necessary but not sufficient, it is a larger window through which we may view a very complex problem, namely network-driven pathogenesis and related therapeutics. Network thinking provides the ability to simplify complex phenomena without losing their essential features; it focuses our attention on the relationship between entities, rather than the entities themselves (for review: Mitchell, 2009). Networks, such as that seen in Fig. 3, mostly exhibit high-clustering and hub structure. These small world networks appear quite efficient because they have short average path lengths between nodes (genes) despite relatively few long-distance links, and thus transfer information quickly at "low cost." *A priori*, such networks display great resilience to the dysfunction of low-degree hubs. Above we present a derived small world network and consider it in the context of CMV-modulated gene message and protein expression (Figs. 3, 5, 6–8).

There is much more to consider in future studies. We have always to remember that small world models are at the last models, that is, constructions based upon simplifying assumptions that may not be entirely congruent with *in vivo* biologic networks. *Problematic assumptions may* include: (a) nodes are functionally identical except for their degree; (b) all links are the same type and have the same potential strength; (c) the published literature upon which the relationships (links) are based contains no false positives or false negatives. Most importantly, drawn networks (*e.g.* Figs. 3, 5) are all

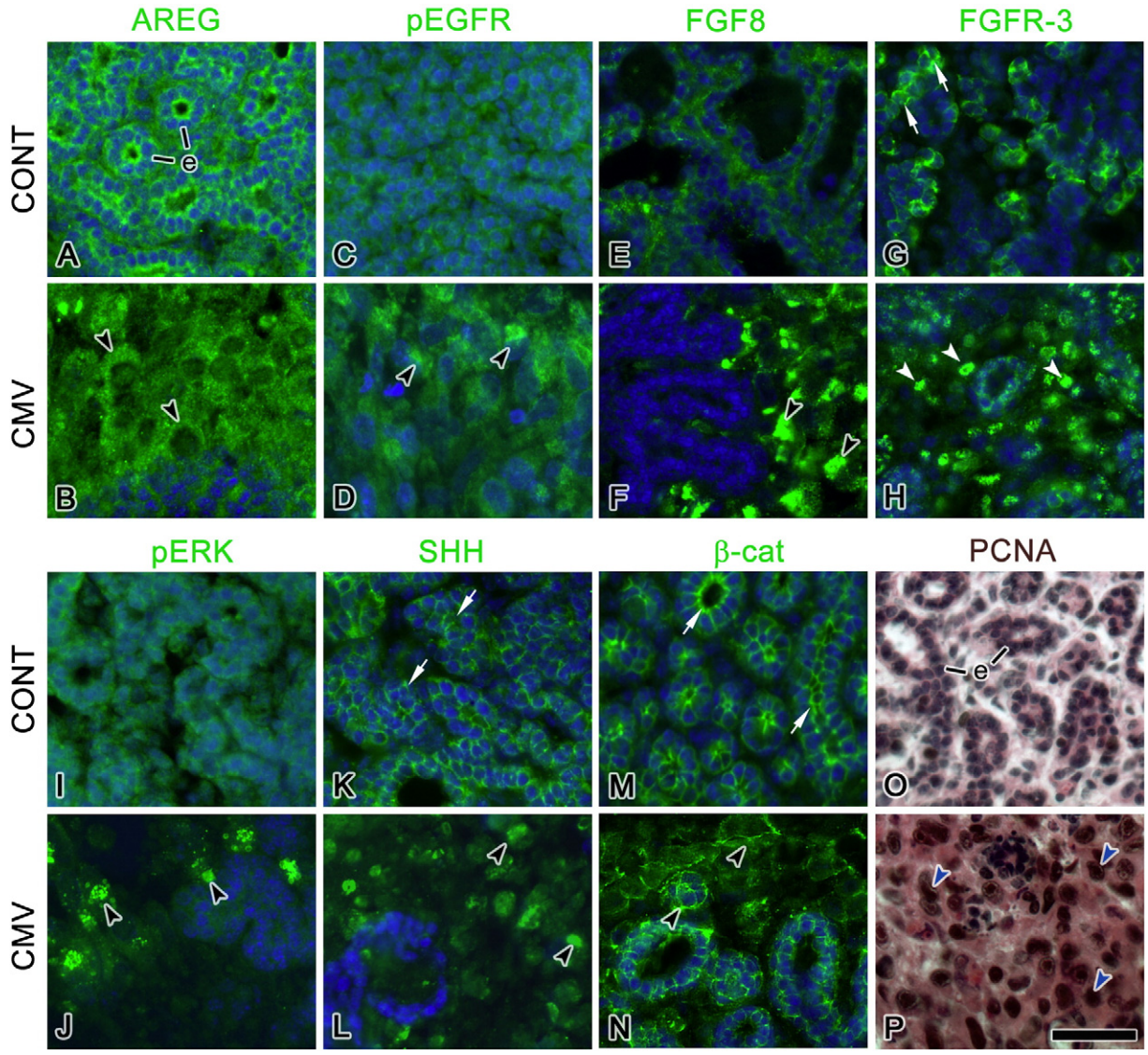

Fig. 7. mCMV-induced stromal localization of components of the AREG/EGFR and FGF8/FGFR3 signaling pathways in NB + 12 SGs. The cell-specific distribution patterns of AREG (A, B), pEGFR (C, D), FGF8 (E, F), pERK (I, J), and SHH (K, L) are similar to those seen in NB + 6 SGs; these proteins are seen throughout abnormal cytomegalic stromal cells (black arrowheads) in mCMV-infected SGs and are relatively absent from controls. G–H. FGFR3 localization. In mCMV-infected SGs, nuclear-localized FGFR3 (H, white arrowheads) is seen in abnormal stromal cells whereas, in controls, membrane-bound FGFR3 is seen (G, white arrows). M–N. β-Catenin localization. In mCMV-infected SGs, β-catenin is found on cell membranes of abnormal stroma (black arrowheads), as well as on the lateral and basal membranes of abnormal epithelia. In contrast, controls exhibit β-catenin on epithelial cell membranes (white arrows), with intense immunostain being seen on lumina-facing membranes (compare N to M). O–P. PCNA localization. There is a notable increase in nuclear-localized PCNA in mCMV-infected SGs (P) compared to controls (O), with nuclear-localized PCNA seen throughout abnormal stroma (blue arrows). In contrast, nuclear-localized PCNA is rarely seen in controls (O). DAPI-stained nuclei appear blue. e—epithelia. Bar, 50 μm.

about the *structure* of the network (static node degree distributions and path length) rather than the dynamics of nonlinear information processing in the context of spatiotemporally evolving node relationships. This is next.

Abbreviations

AREG	amphiregulin
CAFs	cancer-associated fibroblasts
CMV	cytomegalovirus
CONT	control
DAPI	4′,6-diamidino-2-phenylindole dihydrochloride
ERK	extracellular signal regulated protein kinases 1 and 2 (ERK1/2)
EGFR	epidermal growth factor receptor
FGF	fibroblast growth factor
FGFR	fibroblast growth factor receptor
GEF	gefitinib
hCMV	human cytomegalovirus
IPA	Ingenuity pathways analysis
mCMV	mouse cytomegalovirus
MEK	mitogen activated protein kinase kinase
NB	newborn
PCNA	proliferating cell nuclear antigen
pEGFR	phosphorylated EGFR
pERK	phosphorylated ERK
PFU	plaque forming units
qRT-PCR	quantitative RT-PCR
SG	salivary gland
SHH	sonic hedgehog
SG	salivary gland
TEM	tumor microenvironment
TK	tyrosine kinase

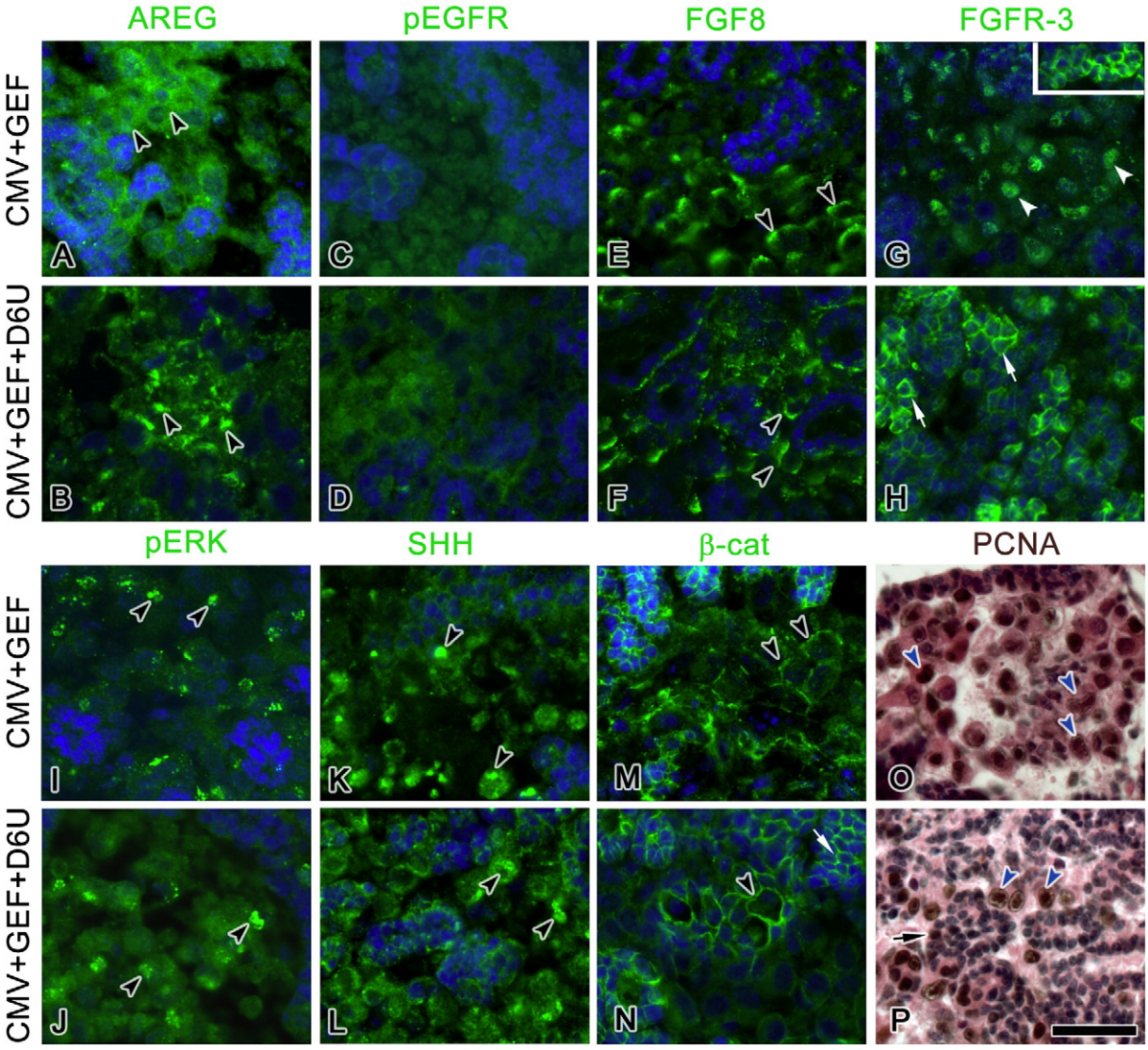

Fig. 8. Effect of GEF-mediated inhibition of EGFR with/without concurrent U0126-mediated inhibition of ERK in NB + 12 mCMV-infected SGs. A, C, E, G, I, K, M, O. In the GEF-treated, mCMV-infected SGs (CMV + GEF), pEGFR is absent (D) and the distribution patterns of AREG (A), pERK (I), SHH (K), β-catenin (M) and nuclear-localized PCNA (O) resemble those seen in untreated, mCMV-infected NB + 12 SGs. There is a marginal decrease in FGF8(E)and nuclear-localized FGFR3 (G, white arrowheads) immunostaining, as well as a notable increase in membrane-bound FGFR3 (G inset) compared to untreated SGs. B, D, F, H, J, L, N, P. In GEF-treated, mCMV-infected SGs treated with U0126 beginning on day 6 (CMV + GEF + D6 U), FGFR3 is membrane (H, white arrows), and not nuclear, localized. Substantial changes in PCNA distribution compared to SGs treated with GEF alone are seen (compare P to O); nuclear-localized PCNA is found in both normal appearing epithelia (black arrow) and in a few abnormal stromal cells (blue arrowheads). The distribution of pERK (J), SHH (L) and β-catenin (N) expression only marginally differs from that seen with GEF treatment alone; β-catenin is also found on epithelial cell membranes (white arrows). DAPI-stained nuclei appear blue. Bar, 50 μm.

Conflict of interest statement

The authors declare that there are no conflicts of interest.

Acknowledgments

We would like to thank Dr. Edward Mocarski for his generous gift of mCMV. This research was supported by the Infectious Disease Fund of the University of Southern California.

References

Aderem, A., Adkins, J.N., Ansong, C., Galagan, J., Kaiser, S., Korth, M.J., Law, G.L., McDermott, J.G., Proll, S.C., Rosenberger, C., Schoolnik, G., Katze, M.G., 2011. A systems biology approach to infectious disease research: innovating the pathogen–host research paradigm. MBio 2 (1), e00325–00310.

Akiyama, R., Kawakami, H., Taketo, M.M., Evans, S.M., Wada, N., Petryk, A., Kawakami, Y., 2014. Distinct populations within Isl1 lineages contribute to appendicular and facial skeletogenesis through the β-catenin pathway. Dev. Biol. 387 (1), 37–48.

Bigelow, R.L., Jen, E.Y., Delehedde, M., Chari, N.S., McDonnell, T.J., 2005. Sonic hedgehog induces epidermal growth factor dependent matrix infiltration in HaCaT keratinocytes. J. Invest. Dermatol. 124 (2), 457–465.

Boppana, S.B., Fowler, K.B., 2007. Persistence in the Population: Epidemiology and Transmission. Cambridge University, Cambridge, MA.

Cerliani, J.P., Vanzulli, S.I., Piñero, C.P., Bottino, M.C., Sahores, A., Nuñez, M., Varchetta, R., Martins, R., Zeitlin, E., Hewitt, S.M., Molinolo, A.A., Lanari, C., Lamb, C.A., 2012. Associated expressions of FGFR-2 and FGFR-3: from mouse mammary gland physiology to human breast cancer. Breast Cancer Res. Treat. 133 (3), 997–1008.

Cortez, E., Roswall, P., Pietras, K., 2014. Functional subsets of mesenchymal cell types in the tumor microenvironment. Semin. Cancer Biol. 25C, 3–9.

Dağ, F., Dölken, L., Holzki, J., Drabig, A., Weingärtner, A., Schwerk, J., Lienenklaus, S., Conte, I., Geffers, R., Davenport, C., Rand, U., Köster, M., Weiß, S., Adler, B., Wirth, D., Messerle, M., Hauser, H., Cičin-Šain, L., 2014. Reversible silencing of cytomegalovirus genomes by type I interferon governs virus latency. PLoS Pathog. 10 (2), e1003962.

Degnin, C.R., Laederich, M.B., Horton, W.A., 2011. Ligand activation leads to regulated intramembrane proteolysis of fibroblast growth factor receptor 3. Mol. Biol. Cell 22 (20), 3861–3873.

Egeblad, M., Nakasone, E.S., Werb, Z., 2010. Tumors as organs: complex tissues that interface with the entire organism. Dev. Cell 18 (6), 884–901.

Engelman, J.A., Settleman, J., 2008. Acquired resistance to tyrosine kinase inhibitors during cancer therapy. Curr. Opin. Genet. Dev. 18 (1), 73–79.

Eswarakumar, V.P., Lax, I., Schlessinger, J., 2005. Cellular signaling by fibroblast growth factor receptors. Cytokine Growth Factor Rev. 16 (2), 139–149.
Giuliani, A., Filippi, S., Bertolaso, M., 2014. Why network approach can promote a new way of thinking in biology. Front. Genet. 5, 83.
Götschel, F., Berg, D., Gruber, W., Bender, C., Eberl, M., Friedel, M., Sonntag, J., Rüngeler, E., Hache, H., Wierling, C., Nietfeld, W., Lehrach, H., Frischauf, A., Schwartz-Albiez, R., Aberger, F., Korf, U., 2013. Synergism between Hedgehog-GLI and EGFR signaling in Hedgehog-responsive human medulloblastoma cells induces downregulation of canonical Hedgehog-target genes and stabilized expression of GLI1. PLoS One 8 (6), e65403.
Hai, B., Yang, Z., Millar, S.E., Choi, Y.S., Taketo, M.M., Nagy, A., Liu, F., 2010. Wnt/β-catenin signaling regulates postnatal development and regeneration of the salivary gland. Stem Cells Dev. 19 (11), 1793–1801.
Han, J.D., Bertin, N., Hao, T., Goldberg, D.S., Berriz, G.F., Zhang, L.V., Dupuy, D., Walhout, A.J., Cusick, M.E., Roth, F.P., Vidal, M., 2004. Evidence for dynamically organized modularity in the yeast protein–protein interaction network. Nature 430 (6995), 88–93.
Hanahan, D., 2014. Rethinking the war on cancer. Lancet 383 (9916), 558–563.
Hanahan, D., Coussens, L.M., 2012. Accessories to the crime: functions of cells recruited to the tumor microenvironment. Cancer Cell 21 (3), 309–322.
Heldin, C.H., 2013. Targeting the PDGF signaling pathway in tumor treatment. Cell Commun. Signal. 11, 97.
Herrera-Abreu, M.T., Pearson, A., Campbell, J., Shnyder, S.D., Knowles, M.A., Ashworth, A., Turner, N.C., 2013. Parallel RNA interference screens identify EGFR activation as an escape mechanism in FGFR3-mutant cancer. Cancer Discov. 3 (9), 1058–1071.
Ho, H.K., Yeo, A.H., Kang, T.S., Chua, B.T., 2014. Current strategies for inhibiting FGFR activities in clinical applications: opportunities, challenges and toxicological considerations. Drug Discov. Today 19 (1), 51–62.
Huang, S., 2011. On the intrinsic inevitability of cancer: from foetal to fatal attraction. Semin. Cancer Biol. 21 (3), 183–199.
Issa, A., Gill, J.W., Heideman, M.R., Sahin, O., Wiemann, S., Dey, J.H., Hynes, N.E., 2013. Combinatorial targeting of FGF and ErbB receptors blocks growth and metastatic spread of breast cancer models. Breast Cancer Res. 15 (1), R8.
Iwatsuki, K., Liu, H.X., Grónder, A., Singer, M.A., Lane, T.F., Grosschedl, R., Mistretta, C.M., Margolskee, R.F., 2007. Wnt signaling interacts with Shh to regulate taste papilla development. Proc. Natl. Acad. Sci. U. S. A. 104 (7), 2253–2258.
Jakob, J.A., Kies, M.S., Glisson, B.S., Kupferman, M.E., Liu, D.D., Lee, J.J., El-Naggar, A.K., Gonzalez-Angulo, A.M., Blumenschein, G.R., 2014. A phase II study of gefitinib in patients with advanced salivary gland cancers. Head Neck. http://dx.doi.org/10.1002/hed.23647.
Jaskoll, T., Leo, T., Witcher, D., Ormestad, M., Astorga, J., Bringas Jr., P., Carlsson, P., Melnick, M., 2004a. Sonic hedgehog signaling plays an essential role during embryonic salivary gland epithelial branching morphogenesis. Dev. Dyn. 229 (4), 722–732.
Jaskoll, T., Witcher, D., Toreno, L., Bringas, P., Moon, A.M., Melnick, M., 2004b. FGF8 dose-dependent regulation of embryonic submandibular salivary gland morphogenesis. Dev. Biol. 268 (2), 457–469.
Jaskoll, T., Abichaker, G., Witcher, D., Sala, F.G., Bellusci, S., Hajihosseini, M.K., Melnick, M., 2005. FGF10/FGFR2b signaling plays essential roles during *in vivo* embryonic submandibular salivary gland morphogenesis. BMC Dev. Biol. 5, 11.
Jaskoll, T., Htet, K., Abichaker, G., Kaye, F.J., Melnick, M., 2011. CRTC1 expression during normal and abnormal salivary gland development supports a precursor cell origin for mucoepidermoid cancer. Gene Expr. Patterns 11 (1–2), 57–63.
Johnston, C.L., Cox, H.C., Gomm, J.J., Coombes, R.C., 1995. Fibroblast growth factor receptors (FGFRs) localize in different cellular compartments. A splice variant of FGFR-3 localizes to the nucleus. J. Biol. Chem. 270 (51), 30643–30650.
Katoh, Y., Katoh, M., 2008. Hedgehog signaling, epithelial-to-mesenchymal transition and miRNA (review). Int. J. Mol. Med. 22 (3), 271–275.
Kirouac, D.C., Du, J.Y., Lahdenranta, J., Overland, R., Yarar, D., Paragas, V., Pace, E., McDonagh, C.F., Nielsen, U.B., Onsum, M.D., 2013. Computational modeling of ERBB2-amplified breast cancer identifies combined ErbB2/3 blockade as superior to the combination of MEK and AKT inhibitors. Sci. Signal. 6 (288), ra68.
Kono, S.A., Marshall, M.E., Ware, K.E., Heasley, L.E., 2009. The fibroblast growth factor receptor signaling pathway as a mediator of intrinsic resistance to EGFR-specific tyrosine kinase inhibitors in non-small cell lung cancer. Drug Resist. Updat. 12 (4–5), 95–102.
Krejci, P., Aklian, A., Kaucka, M., Sevcikova, E., Prochazkova, J., Masek, J.K., Mikolka, P., Pospisilova, T., Spoustova, T., Weis, M., Paznekas, W.A., Wolf, J.H., Gutkind, J.S., Wilcox, W.R., Kozubik, A., Jabs, E.W., Bryja, V., Salazar, L., Vesela, I., Balek, L., 2012. Receptor tyrosine kinases activate canonical WNT/β-catenin signaling via MAP kinase/LRP6 pathway and direct β-catenin phosphorylation. PLoS One 7 (4), e35826.
Lieberman, P.M., 2014. Virology. Epstein–Barr virus turns 50. Science 343 (6177), 1323–1325.
Lujan, B., Hakim, S., Moyano, S., Nadal, A., Caballero, M., Diaz, A., Valera, A., Carrera, M., Cardesa, A., Alos, L., 2010. Activation of the EGFR/ERK pathway in high-grade mucoepidermoid carcinomas of the salivary glands. Br. J. Cancer 103 (4), 510–516.
Marsh, T., Pietras, K., McAllister, S.S., 2013. Fibroblasts as architects of cancer pathogenesis. Biochim. Biophys. Acta 1832 (7), 1070–1078.
Marshall, M.E., Hinz, T.K., Kono, S.A., Singleton, K.R., Bichon, B., Ware, K.E., Marek, L., Frederick, B.A., Raben, D., Heasley, L.E., 2011. Fibroblast growth factor receptors are components of autocrine signaling networks in head and neck squamous cell carcinoma cells. Clin. Cancer Res. 17 (15), 5016–5025.
Mavila, N., James, D., Utley, S., Cu, N., Coblens, O., Mak, K., Rountree, C.B., Kahn, M., Wang, K.S., 2012. Fibroblast growth factor receptor-mediated activation of AKT–β-catenin–CBP pathway regulates survival and proliferation of murine hepatoblasts and hepatic tumor initiating stem cells. PLoS One 7 (11), e50401.
Melnick, M., Jaskoll, T., 2000. Mouse submandibular gland morphogenesis: a paradigm for embryonic signal processing. Crit. Rev. Oral Biol. Med. 11 (2), 199–215.
Melnick, M., Mocarski, E.S., Abichaker, G., Huang, J., Jaskoll, T., 2006. Cytomegalovirus-induced embryopathology: mouse submandibular salivary gland epithelial–mesenchymal ontogeny as a model. BMC Dev. Biol. 6, 42.
Melnick, M., Phair, R.D., Lapidot, S.A., Jaskoll, T., 2009. Salivary gland branching morphogenesis: a quantitative systems analysis of the Eda/Edar/NFkappaB paradigm. BMC Dev. Biol. 9, 32.
Melnick, M., Abichaker, G., Htet, K., Sedghizadeh, P., Jaskoll, T., 2011. Small molecule inhibitors of the host cell COX/AREG/EGFR/ERK pathway attenuate cytomegalovirus-induced pathogenesis. Exp. Mol. Pathol. 91 (1), 400–410.
Melnick, M., Sedghizadeh, P.P., Allen, C.M., Jaskoll, T., 2012. Human cytomegalovirus and mucoepidermoid carcinoma of salivary glands: cell-specific localization of active viral and oncogenic signaling proteins is confirmatory of a causal relationship. Exp. Mol. Pathol. 92 (1), 118–125.
Melnick, M., Deluca, K.A., Sedghizadeh, P.P., Jaskoll, T., 2013a. Cytomegalovirus-induced salivary gland pathology: AREG, FGF8, TNF-α, and IL-6 signal dysregulation and neoplasia. Exp. Mol. Pathol. 94 (2), 386–397.
Melnick, M., Sedghizadeh, P.P., Deluca, K.A., Jaskoll, T., 2013b. Cytomegalovirus-induced salivary gland pathology: resistance to kinase inhibitors of the upregulated host cell EGFR/ERK pathway is associated with CMV-dependent stromal overexpression of IL-6 and fibronectin. Herpesviridae 4, 1.
Mitchell, M., 2009. Complexity: A Guided Tour. Oxford University Press, New York.
Mora, A., Taranta, M., Zaki, N., Badidi, E., Cinti, C., Capobianco, E., 2014. Ensemble inference by integrative cancer networks. Front. Genet. 5, 59.
Nichols, W.G., Boeckh, M., 2000. Recent advances in the therapy and prevention of CMV infections. J. Clin. Virol. 16 (1), 25–40.
Oliveras-Ferraros, C., Cufí, S., Queralt, B., Vazquez-Martin, A., Martin-Castillo, B., de Llorens, R., Bosch-Barrera, J., Brunet, J., Menendez, J.A., 2012. Cross-suppression of EGFR ligands amphiregulin and epiregulin and de-repression of FGFR3 signalling contribute to cetuximab resistance in wild-type KRAS tumour cells. Br. J. Cancer 106 (8), 1406–1414.
Onnela, J.P., 2014. Physics. Flow of control in networks. Science 343 (6177), 1325–1326.
Patel, N., Sharpe, P.T., Miletich, I., 2011. Coordination of epithelial branching and salivary gland lumen formation by Wnt and FGF signals. Dev. Biol. 358 (1), 156–167.
Pietras, K., Ostman, A., 2010. Hallmarks of cancer: interactions with the tumor stroma. Exp. Cell Res. 316 (8), 1324–1331.
Reid, B.S., Yang, H., Melvin, V.S., Taketo, M.M., Williams, T., 2011. Ectodermal Wnt/β-catenin signaling shapes the mouse face. Dev. Biol. 349 (2), 261–269.
Reinchisi, G., Parada, M., Lois, P., Oyanadel, C., Shaughnessy, R., Gonzalez, A., Palma, V., 2013. Sonic hedgehog modulates EGFR dependent proliferation of neural stem cells during late mouse embryogenesis through EGFR transactivation. Front. Cell. Neurosci. 7, 166.
Robinson, K.W., Sandler, A.B., 2013. EGFR tyrosine kinase inhibitors: difference in efficacy and resistance. Curr. Oncol. Rep. 15 (4), 396–404.
Ruths, J., Ruths, D., 2014. Control profiles of complex networks. Science 343 (6177), 1373–1376.
Schwarz, S., Stiegler, C., Müller, M., Ettl, T., Brockhoff, G., Zenk, J., Agaimy, A., 2011. Salivary gland mucoepidermoid carcinoma is a clinically, morphologically and genetically heterogeneous entity: a clinicopathological study of 40 cases with emphasis on grading, histological variants and presence of the t(11;19) translocation. Histopathology 58 (4), 557–570.
Sinor-Anderson, A., Lillien, L., 2011. Akt1 interacts with epidermal growth factor receptors and hedgehog signaling to increase stem/transit amplifying cells in the embryonic mouse cortex. Dev. Neurobiol. 71 (9), 759–771.
Su, W., Meng, F., Huang, L., Zheng, M., Liu, W., Sun, H., 2012. Sonic hedgehog maintains survival and growth of chronic myeloid leukemia progenitor cells through β-catenin signaling. Exp. Hematol. 40 (5), 418–427.
Sütterlin, P., Williams, E.J., Chambers, D., Saraf, K., von Schack, D., Reisenberg, M., Doherty, P., Williams, G., 2013. The molecular basis of the cooperation between EGF, FGF and eCB receptors in the regulation of neural stem cell function. Mol. Cell. Neurosci. 52, 20–30.
Wagner, R.P., Tian, H., McPherson, M.J., Latham, P.S., Orenstein, J.M., 1996. AIDS-associated infections in salivary glands: autopsy survey of 60 cases. Clin. Infect. Dis. 22 (2), 369–371.
Wang, Y., Song, L., Zhou, C.J., 2011. The canonical Wnt/β-catenin signaling pathway regulates Fgf signaling for early facial development. Dev. Biol. 349 (2), 250–260.
Wang, Y.N., Lee, H.H., Lee, H.J., Du, Y., Yamaguchi, H., Hung, M.C., 2012. Membrane-bound trafficking regulates nuclear transport of integral epidermal growth factor receptor (EGFR) and ErbB-2. J. Biol. Chem. 287 (20), 16869–16879.
Ware, K.E., Marshall, M.E., Heasley, L.R., Marek, L., Hinz, T.K., Hercule, P., Helfrich, B.A., Doebele, R.C., Heasley, L.E., 2010. Rapidly acquired resistance to EGFR tyrosine kinase inhibitors in NSCLC cell lines through de-repression of FGFR2 and FGFR3 expression. PLoS One 5 (11), e14117.
Ware, K.E., Hinz, T.K., Kleczko, E., Singleton, K.R., Marek, L.A., Helfrich, B.A., Cummings, C.T., Graham, D.K., Astling, D., Tan, A.C., Heasley, L.E., 2013. A mechanism of resistance to gefitinib mediated by cellular reprogramming and the acquisition of an FGF2–FGFR1 autocrine growth loop. Oncogenesis 2, e39.
Watts, D.J., Strogatz, S.H., 1998. Collective dynamics of 'small-world' networks. Nature 393 (6684), 440–442.
Wilson, T.R., Fridlyand, J., Yan, Y., Penuel, E., Burton, L., Chan, E., Peng, J., Lin, E., Wang, Y., Sosman, J., Ribas, A., Li, J., Moffat, J., Sutherlin, D.P., Koeppen, H., Merchant, M., Neve, R., Settleman, J., 2012. Widespread potential for growth-factor-driven resistance to anticancer kinase inhibitors. Nature 487 (7408), 505–509.

Wiseman, B.S., Werb, Z., 2002. Stromal effects on mammary gland development and breast cancer. Science 296 (5570), 1046–1049.
Young, L.S., Rickinson, A.B., 2004. Epstein–Barr virus: 40 years on. Nat. Rev. Cancer 4 (10), 757–768.
Yuan, J., Liu, X., Wu, A.W., McGonagill, P.W., Keller, M.J., Galle, C.S., Meier, J.L., 2009. Breaking human cytomegalovirus major immediate-early gene silence by vasoactive intestinal peptide stimulation of the protein kinase A-CREB-TORC2 signaling cascade in human pluripotent embryonal NTera2 cells. J. Virol. 83 (13), 6391–6403.
Zammit, C., Barnard, R., Gomm, J., Coope, R., Shousha, S., Coombes, C., Johnston, C., 2001. Altered intracellular localization of fibroblast growth factor receptor 3 in human breast cancer. J. Pathol. 194 (1), 27–34.